

飞秒激光制备蛋白质智能软体执行器

胡昕宇¹, 马卓晨¹, 韩冰², 李春赫¹, 张永来^{1*}¹吉林大学电子科学与工程学院, 集成光电子学国家重点实验室, 吉林 长春 130012;²清华大学精密仪器系, 精密测试技术及仪器国家重点实验室, 北京 100084

摘要 近年来,由柔软和自适应性强的材料组成的智能软体执行器以其高灵活性、生物兼容性和对高负载的机械弹性等一系列优势引起了人们的广泛关注。在各种制造技术中,飞秒激光双光子聚合技术已被证明是一种强有力的工具,促进了智能执行器支持的功能性微机械的发展。利用飞秒激光双光子聚合技术制备了一种基于蛋白质生物材料的对 pH 刺激响应的微机械,一步实现了蛋白质材料的三维构型和内部交联网络密度的三维分布,通过切换溶液的 pH 值实现了生物微机械“手臂”的捕捉和释放动作。这种制备策略在面向生物检测、细胞操控的器件研制方面具有广阔的应用前景。

关键词 激光技术;飞秒激光;软体执行器;pH 响应;蛋白质微纳结构;微机械

中图分类号 TN249

文献标志码 A

doi: 10.3788/CJL202148.1402001

1 引言

近年来,智能执行器件取得了突破性进展,并在显微外科手术、细胞操作^[1-2]和生物传感^[3]等领域显示出了巨大的应用潜力。传统的执行器大多是由刚性材料^[4-6](如金属、硅和二氧化硅)组成的机电一体化系统,因此其生物相容性、柔软性、灵活性和生物降解性较差,限制了它们在生物医学领域的应用。由柔软、自适应性强的材料组成的智能软体执行器展现出了强大的吸引力。与硬体执行器件不同,软体执行器通常基于低杨氏模量的智能材料制造而成,具有高灵活性和生物兼容性,并对高负载具有一定的机械弹性。此外,智能软体执行器可以由各种外部刺激(例如,电、磁^[7-8]、光^[9-11]、热^[12]、pH 值^[13-15]、湿度^[16-17]和化学梯度^[18]等)驱动,通过这些刺激,智能软体执行器无需耦合额外的供能系统就可以实现可预测的变形和可控制的运动。上述优点使得智能软体执行器有望用于精确的体内/体外手术,例如单细胞操作、靶向药物输送和微创手术。

随着微纳加工技术^[19]的进步以及新型材料的发展,小型化、便携化和智能化的产品发展迅猛,并

在各个领域发挥着独特的优势。智能微纳器件已从实现简单的机动性发展到功能性,后续可进一步发展到可编程化和 4D 变形化,最终有望实现智能机器人的制造。目前,人们已经利用各种软体材料成功制备了具有多种功能的执行器,例如:Wu 等^[20]利用多光束干涉技术制造了可控的三维微结构阵列,其在溶液调控下能自由可逆地捕获和释放粒子;Lee 等^[21]借助 3D 打印技术制备了大容量 O 型磁选机的圆柱形三维微通道,加强和完善了新型免疫磁流分析技术。对未来的智能软体执行器而言,利用生物相容性材料进行制备具有极大的优势,可将其直接应用于细胞操作、组织切片等生物医学应用。因此,研究如何利用生物相容性材料制备智能软体执行器极其重要,对于开发诸如智能微型机器人和微机械系统等具有重要意义^[22]。

本文基于生物相容性好的牛血清白蛋白(BSA)使用飞秒激光双光子聚合技术成功制备了一种三维微机械。该器件采用的是密度不均匀的网格结构,因为目前的智能材料一般是对固有刺激具有响应的材料或多层材料的组装。在外界刺激下,前者由于化学键或分子结构重排而变形,后者则由于不同层

收稿日期: 2021-01-06; 修回日期: 2021-01-22; 录用日期: 2021-02-18

基金项目: 国家重点研发计划(2017YFB1104600)、国家自然科学基金(61935008,61775078,61905087,61590930)、吉林省科技发展规划(20180101061JC)

通信作者: *yonglaizhang@jlu.edu.cn

间的应力失配而变形。然而,它们在应用中都存在着一些问题,如三维成形、各向同性变形以及与其他器件的集成。飞秒激光以其强大的三维加工能力,可在实现微纳器件外部轮廓三维直写的同时调控结构内部材料的特性。基于上述设计策略,本课题组通过测试外部环境刺激下微机械的膨胀程度与弯曲角度、网格密度大小之间的关系,进一步设计制作了具有捕捉和释放能力的三维机械手臂模型。本文的设计策略在未来的生物医学工程^[23-24]、光学系统^[25-26]、微机械系统^[27]、化学分析^[28]等领域具有广阔的应用前景。

2 蛋白质微纳器件的飞秒激光制备

2.1 基于蛋白质材料的光刻胶

基于蛋白质材料 BSA 的光刻胶具有生物相容性好、柔性高等特点,并且由于 BSA 分子链中存在

羧基和氨基,在高于或低于等电点的酸碱溶液中 BAS 会产生去质子化或质子化,静电排斥作用加强,导致 BAS 发生结构膨胀。本文使用 BSA 作为单体,MB(亚甲基蓝)作为光引发剂按一定配比混合形成实验所用的光刻胶。首先,将适量 BSA 和亚甲基蓝溶解在超纯水(电阻率为 $18.2 \text{ M}\Omega \cdot \text{cm}$, $25 \text{ }^\circ\text{C}$)中,形成由 500 mg/mL BSA 和 0.6 mg/mL 亚甲基蓝组成的黏性蛋白质水凝胶;然后,将制备好的凝胶在 $4 \text{ }^\circ\text{C}$ 暗箱中孵育 24 h ,使组成物质充分溶解。本文拟通过探索凝胶的膨胀比与交联密度的关系,开发一种材料相同但交联密度不同的双层微机械。原理图如图 1 所示,微机械悬臂由两层交联密度不同的材料制备而成,当切换溶液的 pH 值时,交联密度不同的材料的膨胀度不同,弯曲的悬臂向内进行抓捕动作或向外完成释放动作,实现自由智能的机械动作行为。

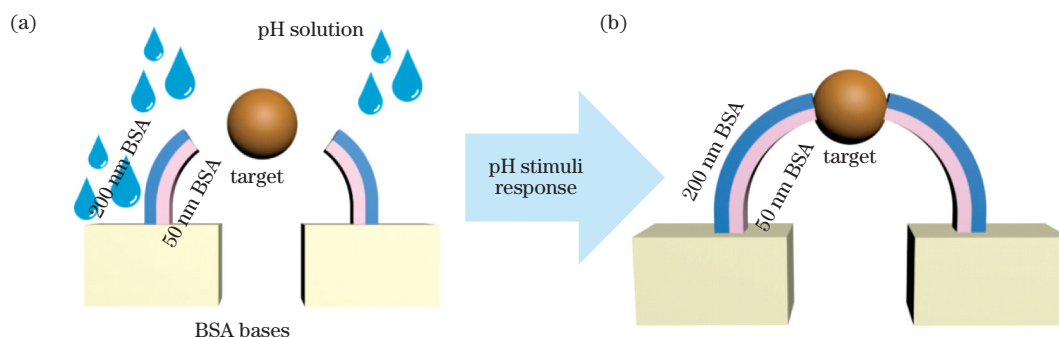


图1 智能微纳器件示意图。(a) pH刺激前智能微机械的原始状态;(b)智能微机械受pH刺激后响应,“抓住”微纳颗粒
Fig.1 Schematics of intelligent micro-nano device. (a) Original state of intelligent micro-machine before pH stimulation; (b) in response to the stimulus of pH, the intelligent micro-machine “grasps” micro-nano particle

2.2 飞秒激光双光子聚合技术

飞秒激光双光子聚合直写具有自由的可编程设计能力、强大的三维处理能力和高空间分辨率等优点,是一种具有无限潜能的微纳加工方法^[29-30]。实验中采用自制的飞秒激光双光子聚合加工系统制备 BSA 微结构。在制作过程中,先将 $20 \mu\text{L}$ 的 BSA 水凝胶滴到玻璃基板上,并使用聚二甲基硅氧烷 (PDMS) 腔来减缓凝胶中水分的蒸发。激光束由一个中心波长为 800 nm 、脉冲宽度为 120 fs 、重复频率为 80 MHz 的 Ti:sapphire 飞秒激光振荡器产生,然后使用 60 倍油浸物镜(数值孔径 $NA = 1.4$) 将飞秒激光紧密聚焦到水凝胶上进行逐点三维扫描。一般情况下,在使用物镜之前测量得到的平均激光功率为 20 mW ,每个体素的曝光时间为 $1000 \mu\text{s}$ 。制作完成后,将样品置于超纯水中显影几分钟,以去除未聚合的水凝胶。飞秒激光双光子聚合技术具有三维悬空加工能力,可以制备高自由度的微机械

结构^[31]。

3 实验结果与讨论

3.1 BSA 微结构的 pH 响应特性

基于蛋白质材料的微纳结构具有明显的 pH 响应,利用其响应特性对蛋白质微结构的膨胀或收缩进行调控对于研究蛋白质的基本性质及其潜在应用具有重要意义。为了探索 pH 响应的具体参数,配制质量浓度为 500 mg/mL 的 BSA 溶液作为实验溶剂。为了探索酸碱环境下激光扫描步长(影响结构交联网络密度)对 BSA 微结构膨胀度的影响,利用飞秒激光双光子聚合技术在玻璃衬底上加工激光扫描步长为 $100, 150, 200 \text{ nm}$ 的三种方块结构,结构的尺寸为 $15 \mu\text{m} \times 15 \mu\text{m} \times 5 \mu\text{m}$ (长 \times 宽 \times 高)。在加工过程中需要注意的是,光刻胶不能在空气中长时间暴露,因为其内部水分会蒸发,导致光刻胶干燥结块,严重影响后续加工。因此,在加工过程中需要

密封。PDMS具有良好的化学稳定性,且与玻璃的键合力较强,因此将PDMS作为密封器件,以有效防止光刻胶变质。接下来将三种扫描步长下制作的方块微结构分别浸入pH值为1、3、5、13的溶液中,观察它们的膨胀情况,并计算出膨胀比。膨胀比的计算公式为

$$P = S_1/S_2, \quad (1)$$

式中: P 为微纳结构浸入不同溶剂后其上表面面积的膨胀比; S_1 为微纳结构浸入不同pH值溶剂后的上表面面积; S_2 为微纳结构浸入pH值为5的溶剂后上表面面积。因为BSA等电位点的pH值约为4.7,所以在pH值为5时,BSA微结构的面积最小,以此时的面积作为参比标准。如图2所示,当激光扫描步长为200 nm时,BSA的膨胀比随着pH从1变化到13呈现先减小后增大的趋势:在pH为1的溶液中,膨胀比约1.9;膨胀比在等电位点处最低;

在pH为13的溶液中,膨胀比高达2.65。内部网格密度越大,采用双光子聚合技术直写的微纳结构越坚固。随着扫描步长从100 nm增大到200 nm,由于结构的交联密度逐渐变小,因而膨胀比呈现出逐渐变大的趋势。由方块在酸碱溶液下的膨胀比可以看出,当扫描步长为100 nm时,方块在碱性溶液中的膨胀比是200 nm扫描步长下的76.7%。将微纳结构浸入pH值为13的溶液中,并用计时器测量其响应时间。从图2(c)中可以看出,随着溶液的pH值由5切换至13,微纳结构的体积迅速膨胀,在约1.5 s后膨胀比达到最大值。为了证明BSA这种材料的稳定性和可重复性,在实验中进行百次响应刺激,结果如图2(d)所示,经历反复多次响应刺激后,该材料依然具有良好的响应行为。由此,本文进一步设计了不同扫描步长的双层BSA结构。

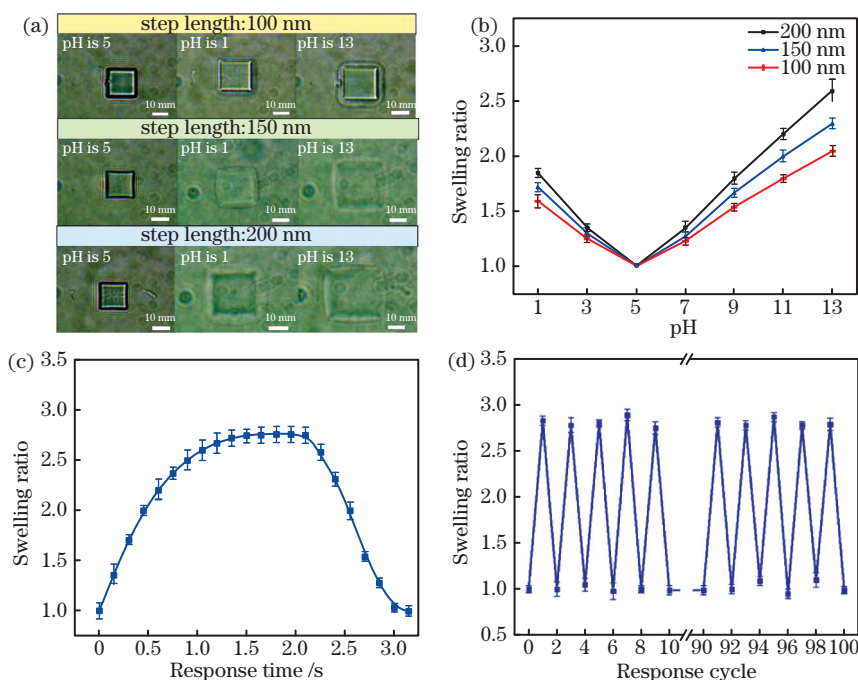


图2 BSA微结构的pH响应特性。(a)三种激光扫描步长(100,150,200 nm)的BSA方块结构($15\ \mu\text{m}\times 15\ \mu\text{m}\times 5\ \mu\text{m}$)在不同pH值溶液中的光学显微镜照片;(b)三种激光扫描步长的BSA结构的膨胀比随pH值的变化;(c)响应时间与膨胀比的关系曲线;(d)在pH值为13的溶液中,百次循环刺激响应与膨胀比之间的关系

Fig. 2 pH-response properties of BSA structures. (a)Optical microscope images of BSA block structure ($15\ \mu\text{m}\times 15\ \mu\text{m}\times 5\ \mu\text{m}$) processed at three scanning step lengths (100, 150, and 200 nm) in solvent with different pH values; (b) variation of swelling rate of BSA structure processed at three step lengths with pH value; (c) relationship between response time and swelling ratio; (d) relationship between swelling to 100 cycles of stimulation and the swelling ratio in a solvent with pH of 13

如图3所示,本课题组加工了内侧与外侧扫描步长不同的方块结构(内侧的扫描步长为100 nm,外侧的扫描步长为200 nm),外侧方块的尺寸为 $10\ \mu\text{m}\times 10\ \mu\text{m}\times 5\ \mu\text{m}$ (长×宽×高),内侧方块的

尺寸为 $5\ \mu\text{m}\times 5\ \mu\text{m}\times 5\ \mu\text{m}$ (长×宽×高)。从方块结构的三维景深共聚焦显微镜照片可以看出,加工的结构完整,同时也可以看出当BSA材料显影之后,由于内外圈的收缩程度不同,原本一个标准的

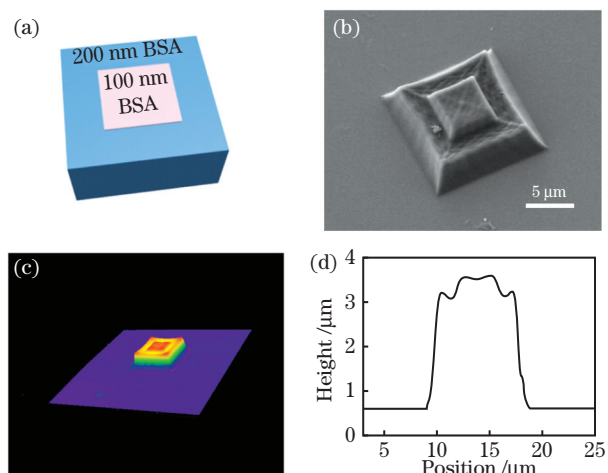


图3 基于BSA的非均匀扫描步长方块结构的制备和表征。(a) BSA方块结构的3DMAX模型图;(b) BSA方块结构的电镜(SEM)图片;(c) BSA方块结构的三维景深共聚焦显微镜图像;(d) BSA方块结构的横截面轮廓

Fig. 3 Fabrication and characterization of BSA-based block structure with non-uniform scanning step lengths. (a) 3DMAX model of BSA block structure; (b) SEM images of BSA block structure; (c) three-dimensional laser confocal microscopy image of BSA-based block structure; (d) cross-sectional profile of BSA-based block structure

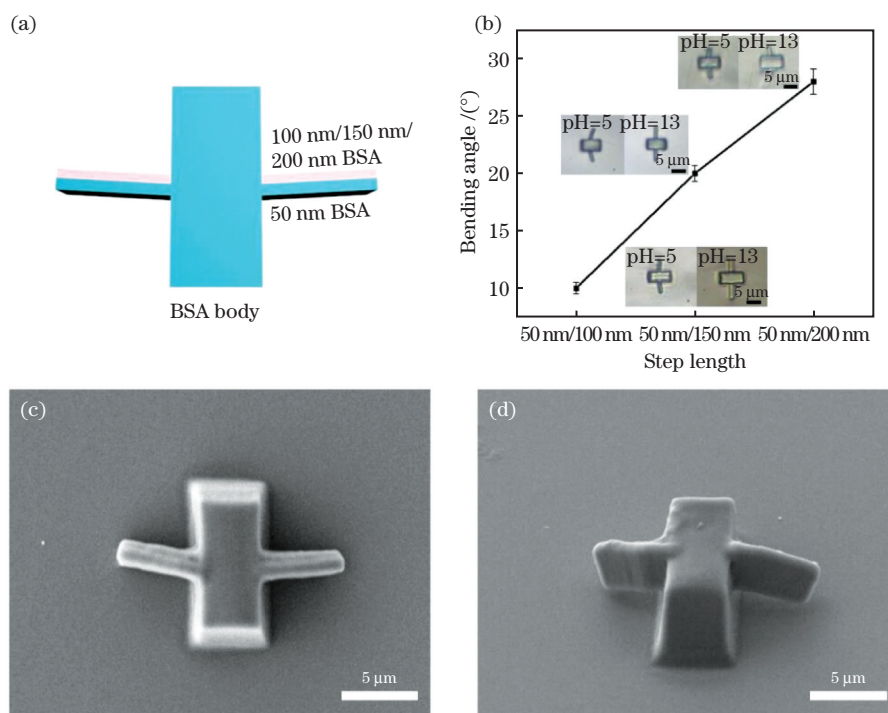


图4 BSA 双层悬臂结构的动态响应。(a) 双层悬臂结构的3DMAX模型图;(b) 悬臂弯曲角度与双层扫描步长的关系;(c) BSA悬臂结构的SEM图;(d) BSA悬臂结构倾斜30°的SEM图

Fig. 4 Dynamic response of BSA-based bilayer cantilever structure. (a) 3DMAX model of bilayer cantilever structure; (b) relationship between cantilever bending angle and double-layer scanning step length; (c) SEM image of BSA-based cantilever structure; (d) SEM image of BSA-based cantilever structure tilted at 30°

方块模型变成了内高外低的凸起结构。从截面图中可以看出,收缩后外侧方块约高 $3 \mu\text{m}$,而内侧方块约高 $3.65 \mu\text{m}$ 。这是因为内部网格密度大的微纳结构的坍塌程度要小于外部网格密度小的微纳结构,即扫描步长大的结构的形变程度或者说收缩比会更大。可以相信,利用该加工方法可以制备出丰富的程序可控的智能微纳器件。

由实验结果可以看出,同材料不同扫描步长的非均匀结构具有很大的应用潜能。本课题组设计了一款双层微纳悬臂,该悬臂外侧层是网格密度较为稀疏的结构,而内侧层是网格密度较为紧密的结构。在外界酸碱溶液的刺激下,外侧层的膨胀度大于内侧层,因此产生的内外应力差导致悬臂结构总体向内弯曲。如图4所示,本课题组利用飞秒激光双光子聚合加工了三种不同扫描步长($50 \text{ nm}/100 \text{ nm}$, $50 \text{ nm}/150 \text{ nm}$, $50 \text{ nm}/200 \text{ nm}$)的双层悬臂结构,悬臂尺寸为 $5 \mu\text{m} \times 4 \mu\text{m} \times 1.6 \mu\text{m}$ (长 \times 宽 \times 厚),双层悬臂结构网格密度较大和较小部分的厚度均为 800 nm ,底座扫描步长为 50 nm 。双层结构的网格密度差越大,在不同 pH 值溶液(pH 值分别为 5 和 13)的刺激下,双层结构的弯曲度越大,弯曲度与扫描步长呈正相关性。但网格密度过大,就会造成结

构脱落、激光制造成形困难等问题。从实验结果可以看出,当双层扫描步长为 50 nm/200 nm 时,双层悬臂结构的转动角度最大,为 28°。由图 4(b)中的插图可以看出:当 pH 值为 5 时,双层结构存在不同程度的向内弯曲,这是因为在显影之后 BSA 会出现少许收缩现象,而扫描步长较大的一侧比扫描步长较小一侧的收缩程度更大一些,因此会造成一定的向内弯曲现象;当 pH 值为 13 时,扫描步长大的一侧发生膨胀,产生了不同程度的反向弯曲,所以悬臂相比 pH 值为 5 时发生了不同角度的转动。考虑到 BSA 蛋白质的良好生物兼容性,这种 pH 调控的智能微纳器件在面向生物的微操作机械中具有一定的应用前景。

3.2 基于 BSA 蛋白质材料的微机械的应用

基于上述研究,本课题组设计了一种基于外界刺激响应完成“抓捕”和“释放”功能的生物相容性材料微机械。利用 3DMAX 软件设计微机械模型,该微机械由两部分组成:尺寸为 10 μm × 6 μm × 5 μm (长 × 宽 × 高)的双底座以及长为 6 μm 、扫描步长为 50 nm/200 nm 的双层悬臂。如图 5(a)所示,将所设计的微机械浸入 pH 值为 13 的溶液中,微机械“手臂”向内弯曲,实现“抓捕”动作;当将溶液的 pH 值切换 5 时,微机械“手臂”恢复原状,实现“释放”动作。接下来,用所设计的微机械捕捉宽为 6 μm 的

微纳棒状结构,从图 5(b)可以明显观察到:当将所设计的微机械浸入 pH 值为 5 溶液时,微机械没有明显反应,且棒状结构与悬臂中间有很大空隙;当将溶液的 pH 值切换至 1 时,微机械“手臂”快速“抓住”微纳棒;当将 pH 值切换为 13 时,微机械“手臂”的膨胀度更大,紧紧“抓住”微纳棒状结构;再次将 pH 值切换至 5,微机械“手臂”快速完成“释放”动作。图 5(c)所示为两悬臂间距与响应时间之间的关系,可以看出:当悬臂受刺激响应后,两悬臂之间的距离变小;约 1 s 后悬臂在 pH 刺激下开始响应,完成向内收缩抓取物体的动作;再经过约 1.2 s 后悬臂打开完成物体的释放。在环境 pH 值循环过程中,蛋白质三维微机械经历了明显的可逆变形。所设计的 BSA 微机械在多次反复刺激下性能没有明显下降,如图 5(d)所示。在实验中将溶液的 pH 值在 5~13 之间切换 100 个周期,结果发现,所设计的微机械依然可以很好地实现“抓捕”和“释放”动作,重复性良好。相比其他硬质材料,如 SU-8 和硅基材料等,由 BSA 制备的微机械可以有效快速地完成动作响应,且这种软体微机械在抓捕细胞类微小物体时,由于其自身的柔软性不会对微小物体造成损坏。本课题组设计的微机械的这种特性使其在细胞微操作、分析以及对 pH 值敏感的生物传感器方面具有潜在应用。

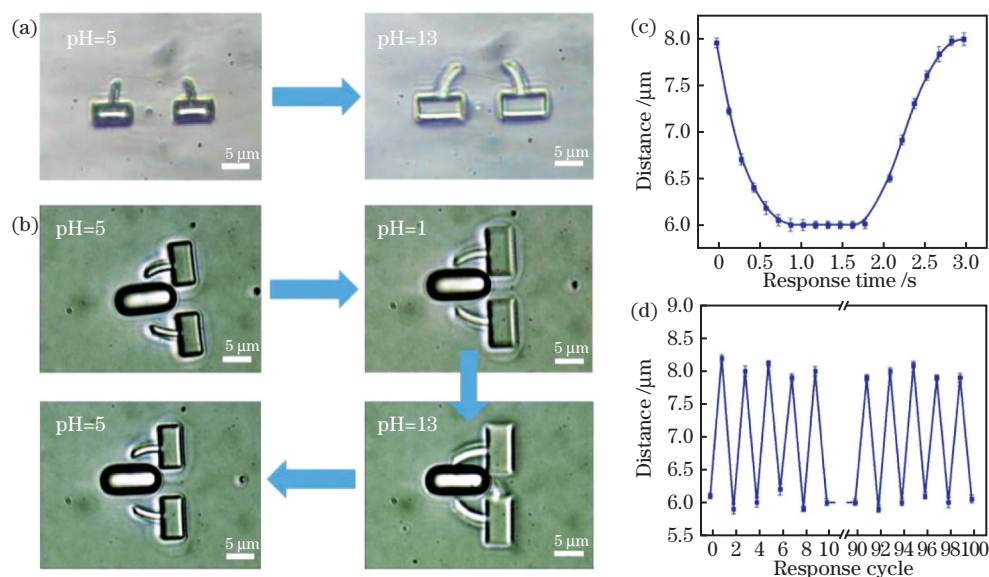


图 5 pH 调控的智能微机械。(a)微机械在 pH 刺激下的响应;(b)智能微机械完成“抓住”“释放”“紧抓”物体的反复可逆动作;(c)微机械悬臂间距与响应时间的关系曲线;(d)微机械悬臂在 pH 值为 5~13 溶液中实现 100 次循环切换

Fig. 5 pH-driven intelligent micro-machine. (a) Responses of micro-machine to pH stimulus; (b) repeated reversible actions of “grasping”, “releasing”, and “grasping tightly” by the intelligent micro-machine; (c) distance between the micro-mechanical cantilever versus response time; (d) micro-mechanical cantilever enables 100 cycles switching in a solvent with pH values of 5 to 13

4 结 论

本文提出了具有 pH 响应的材料内部为非均匀网格密度的微机械的制备策略,并利用飞秒激光双光子聚合技术制备了精度高的三维微纳器件。通过探索 BSA 生物材料的 pH 响应特性,进一步展示了通过所提策略实现了具有选择性且能精确快速完成捕获、释放动作的软体智能微机械。随着新型制造方案和功能材料的快速发展,具有丰富和前所未有的智能微纳器件的构建可以高效地进行。毫无疑问,在先进激光集成技术的帮助下,这种利用生物相容性好的蛋白质材料制作的智能微机械在未来的生物医学检测、微细胞分析和仿生学等领域将发挥越来越重要的作用。

参 考 文 献

- [1] Hu K, Yang L, Jin D D, et al. Tunable microfluidic device fabricated by femtosecond structured light for particle and cell manipulation [J]. *Lab on a Chip*, 2019, 19(23): 3988-3996.
- [2] Wu D, Wang J N, Wu S Z, et al. Three-level biomimetic rice-leaf surfaces with controllable anisotropic sliding [J]. *Advanced Functional Materials*, 2011, 21(15): 2927-2932.
- [3] Kelemen L, Lepera E, Horváth B, et al. Direct writing of optical microresonators in a lab-on-a-chip for label-free biosensing [J]. *Lab on a Chip*, 2019, 19(11): 1985-1990.
- [4] Kenis P J, Ismagilov R F, Whitesides G M. Microfabrication inside capillaries using multiphase laminar flow patterning [J]. *Science*, 1999, 285(5424): 83-85.
- [5] Yin D, Feng J, Ma R, et al. Efficient and mechanically robust stretchable organic light-emitting devices by a laser-programmable buckling process [J]. *Nature Communications*, 2016, 7: 11573.
- [6] Yin D, Jiang N R, Liu Y F, et al. Mechanically robust stretchable organic optoelectronic devices built using a simple and universal stencil-pattern transferring technology [J]. *Light, Science & Applications*, 2018, 7: 35.
- [7] Xia H, Wang J, Tian Y, et al. Ferrofluids for fabrication of remotely controllable micro-nanomachines by two-photon polymerization [J]. *Advanced Materials*, 2010, 22(29): 3204-3207.
- [8] Tian Y, Zhang Y L, Xia H, et al. Solvent response of polymers for micromachine manipulation [J]. *Physical Chemistry Chemical Physics*, 2011, 13(11): 4835-4838.
- [9] Hippler M, Blasco E, Qu J, et al. Controlling the shape of 3D microstructures by temperature and light [J]. *Nature Communications*, 2019, 10(1): 232.
- [10] Yuan H W, Rao S L, Wu D, et al. Fabrication and rotation driving of movable microstructures based on femtosecond laser [J]. *Optics and Precision Engineering*, 2020, 28(3): 584-590.
袁宏伟, 饶生龙, 吴东, 等. 基于飞秒激光的可运动微结构加工与旋转驱动 [J]. *光学精密工程*, 2020, 28(3): 584-590.
- [11] Ding R, Wang X P, Feng J, et al. Clarification of the molecular doping mechanism in organic single-crystalline semiconductors and their application in color-tunable light-emitting devices [J]. *Advanced Materials*, 2018, 30(43): e1801078.
- [12] Bi Y G, Feng J, Li Y F, et al. Broadband light extraction from white organic light-emitting devices by employing corrugated metallic electrodes with dual periodicity [J]. *Advanced Materials*, 2013, 25(48): 6969-6974.
- [13] Jeong B, Gutowska A. Lessons from nature: stimuli-responsive polymers and their biomedical applications [J]. *Trends in Biotechnology*, 2002, 20(7): 305-311.
- [14] Ma Z C, Zhang Y L, Han B, et al. Femtosecond laser programmed artificial musculoskeletal systems [J]. *Nature Communications*, 2020, 11(1): 4536.
- [15] Sun R, Wang C Y, Hu Y L, et al. Processing and application of hydrogel Janus micropillars based on femtosecond laser [J]. *Chinese Journal of Lasers*, 2019, 46(9): 0902001.
孙锐, 王重宇, 胡衍雷, 等. 飞秒激光加工水凝胶双面神微柱及其应用 [J]. *中国激光*, 2019, 46(9): 0902001.
- [16] Lv C, Sun X C, Xia H, et al. Humidity-responsive actuation of programmable hydrogel microstructures based on 3D printing [J]. *Sensors and Actuators B*, 2018, 259: 736-744.
- [17] Han D D, Zhang Y L, Ma J N, et al. Sunlight-reduced graphene oxides as sensitive moisture sensors for smart device design [J]. *Advanced Materials Technologies*, 2017, 2(8): 1700045.
- [18] Ueki T. Stimuli-responsive polymers in ionic liquids [J]. *Polymer Journal*, 2014, 46(10): 646-655.
- [19] Li Z Z, Wang L, Fan H, et al. O-FIB: far-field-induced near-field breakdown for direct nanowriting in an atmospheric environment [J]. *Light, Science & Applications*, 2020, 9: 41.
- [20] Wu D, Wu S Z, Zhao S, et al. Rapid, controllable fabrication of regular complex microarchitectures by

- capillary assembly of micropillars and their application in selectively trapping/releasing microparticles[J]. *Small*, 2013, 9(5): 760-767.
- [21] Lee W, Kwon D, Chung B, et al. Ultrarapid detection of pathogenic bacteria using a 3D immunomagnetic flow assay [J]. *Analytical Chemistry*, 2014, 86(13): 6683-6688.
- [22] Zhang Y L, Tian Y, Wang H, et al. Dual-3D femtosecond laser nanofabrication enables dynamic actuation[J]. *ACS Nano*, 2019, 13(4): 4041-4048.
- [23] Sun Y L, Dong W F, Yang R Z, et al. Dynamically tunable protein microlenses[J]. *Angewandte Chemie International Edition*, 2012, 51(7): 1558-1562.
- [24] Sun Y L, Dong W F, Niu L G, et al. Protein-based soft micro-optics fabricated by femtosecond laser direct writing [J]. *Light: Science & Applications*, 2014, 3(1): e129.
- [25] Zou X J, Zheng G G, Yuan Q, et al. Imaging based on metalenses[J]. *PhotonIX*, 2020, 1(1): 1-24.
- [26] Wu D, Chen Q D, Niu L G, et al. Femtosecond laser rapid prototyping of nanoshells and suspending components towards microfluidic devices[J]. *Lab on a Chip*, 2009, 9(16): 2391-2394.
- [27] Gu C L, Zuo Z, Luo D P, et al. Passive coherent dual-comb spectroscopy based on optical-optical modulation with free running lasers [J]. *PhotonIX*, 2020, 1(1): 1-9.
- [28] Xu B B, Zhang Y L, Xia H, et al. Fabrication and multifunction integration of microfluidic chips by femtosecond laser direct writing[J]. *Lab on a Chip*, 2013, 13(9): 1677-1690.
- [29] Sugioka K, Cheng Y. Ultrafast lasers: reliable tools for advanced materials processing[J]. *Light: Science & Applications*, 2014, 3(4): e149.
- [30] Sergeev A A, Pavlov D V, Kuchmizhak A A, et al. Tailoring spontaneous infrared emission of HgTe quantum dots with laser-printed plasmonic arrays[J]. *Light: Science & Applications*, 2020, 9: 16.
- [31] Hu W J, Xu B, Shi Y, et al. Flow sensor with high sensitivity fabricated by femtosecond laser [J]. *Chinese Journal of Lasers*, 2018, 45(9): 0902001. 胡文锦, 许兵, 史杨, 等. 飞秒激光制备高敏感度流量传感器[J]. *中国激光*, 2018, 45(9): 0902001.

Femtosecond Laser Fabrication of Protein-Based Smart Soft Actuators

Hu Xinyu¹, Ma Zhuochen¹, Han Bing², Li Chunhe¹, Zhang Yonglai¹

¹ State Key Laboratory of Integrated Optoelectronics, College of Electronic Science and Engineering, Jilin University, Changchun, Jilin 130012, China;

² State Key Laboratory of Precision Testing Technology and Instruments, Department of Precision Instruments, Tsinghua University, Beijing 100084, China

Abstract

Objective In recent years, significant progress has been made in smart actuation devices; they have great potential for applications in microsurgery, cell manipulation, and biosensing. The majority of conventional actuators are mechatronic devices made of hard materials (e.g., metals, silicon, and silica) with low biocompatibility, softness, flexibility, and biodegradability, limiting their use in biomedical domains. Therefore, smart soft actuators made of soft and adaptive materials have significant advantages in this area. Biocompatible materials that can be directly applied to biomedical applications, such as cell manipulation and tissue sectioning, have significant advantages for future smart soft actuators. Thus, studying the treatment of biocompatible materials to create smart soft actuators critical for the development of intelligent micro-robots and micromechanical systems is crucial. In this paper, three-dimensional (3D) micromechanical structures based on biocompatible BSA (bovine serum albumin) material are directly written using the femtosecond laser two-photon polymerization technique. The femtosecond laser's high 3D processing capabilities allow for 3D direct writing of the micro-nano devices' external contours while modulating the properties of the materials inside the structure. The relationship between the degree of micromechanical expansion under external environmental stimulation and the bending angle, as well as the size of the mesh density, is examined using the design technique presented in this research. Furthermore, a 3D robotic arm model with capture and release capability is designed and fabricated. In the future, this design approach will have numerous applications in biomedical engineering, optical systems, micromechanical systems, and other domains.

Methods In this study, BSA serves as the monomer, and MB (methylene blue) serves as the photoinitiator for the experiments. To make a viscous protein hydrogel, 500 mg/mL BSA and 0.6 mg/mL MB were dissolved in ultrapure water (18.2 M Ω ·cm, 25 °C). The prepared gels were then incubated at 4 °C for 24 h in a dark box to completely dissolve the constituent components. A homemade femtosecond laser two-photon polymerization processing equipment was used to obtain the BSA microstructures. For the fabrication, 20 μ L BSA hydrogel was charged into a glass substrate, and a PDMS (polydimethylsiloxane) cavity was used to limit the evaporation of water in the gel. A Ti:sapphire femtosecond laser oscillator (Spectra-Physics 3960-X1BB) with a central wavelength of 800 nm, a pulse width of 120 fs, and an 80 MHz repetition rate generate the laser beam. A 60 \times oil immersion objective is employed to concentrate the femtosecond laser closely into the hydrogel for point-by-point 3D scanning. Before employing the objective, 20 mW-average laser power was measured, and the exposure duration for each voxel was 1000 μ s. The samples were thoroughly rinsed in ultrapure water for few minutes after fabrication to remove the unpolymerized hydrogel.

Results and Discussions The swelling ratio of BSA micro-nano blocks increased as the scanning step length increased from 100 nm to 200 nm because of a decrease in the cross-linking density of the processed structures. In a pH 1 solution, the swelling ratio is about 1.9 when the step length is 200 nm, whereas in a pH 13 solution, the swelling ratio is 2.65. For a step length of 100 nm in an alkaline solution, the swelling ratio is 76.7% of a 200 nm step length fabricated structure. In this paper, femtosecond laser two-photon polymerization was used to fabricate three bilayer cantilever structures with different scan step length distributions of 50 nm/100 nm, 50 nm/150 nm, and 50 nm/200 nm. According to the experimental results, the maximum rotation angle of the bilayer cantilever structure is 28° when the bilayer scanning step length is 50 nm/200 nm. As shown in Figure 5 (b), the micro-machine was subsequently employed to capture a micro-nano rod structure with a width of 6 μ m. When switched to the solution with pH 13, the micromechanical “arm” swells and “grip” the rod tightly. The “release” operation can be completed quickly by switching back to the pH 5 solution. The experiment can be repeated over and over again.

Conclusions This work describes a method for fabricating micromechanical devices using pH-responsive materials with nonuniform internal lattice density. Here, 3D micro-nano devices with high precision can be flexibly designed and produced using a femtosecond laser two-photon polymerization technique. It is also demonstrated that soft smart micro-machine with selective and accurate trapping and releasing may be obtained utilizing this technique by investigating the pH-responsive characteristics of BSA biomaterials. The construction of smart micro-nano devices with extensive and unprecedented functionality can be easily accomplished due to the rapid development of novel fabrication techniques and functional materials. Such smart micro-machines produced from biocompatible protein materials will play an essential role in future applications such as biomedical detection, microcellular analysis, and bionanotechnology because of advanced laser integration technology.

Key words laser technique; femtosecond laser; soft actuator; pH response; protein microstructures; micro-machine

OCIS codes 140.3390; 190.7110; 220.4000; 160.1435